7304 *Inorg. Chem.* **2010**, *49*, 7304–7312
DOI: 10.1021/ic1002989

Inorganic Chemistry
Article

Zinc, Cadmium, and Mercury Complexes with Fluorinated Selenolate Ligands

Thomas J. Emge,* Michael D. Romanelli, Brian F. Moore, and John G. Brennan*

Department of Chemistry and Chemical Biology, Rutgers, The State University of New Jersey, 610 Taylor Road, Piscataway, New Jersey 08854-8087

Received February 12, 2010

Reductive cleavage of $C_6F_5SeSeC_6F_5$ with elemental M (M = Zn, Cd, and Hg) in pyridine results in the formation of $(py)_2Zn(SeC_6F_5)_2$, $(py)_2Cd(SeC_6F_5)_2$, and $Hg(SeC_6F_5)_2$. Structural characterization of the Zn and Cd compounds reveals tetrahedral coordination environments, while the Hg compound shows a complicated series of linear structures with two short, nearly linear Hg−Se bonds, up to two longer and perpendicular Hg···Se interactions, and no coordinated pyridine ligands. All three compounds exhibit well-defined intermolecular $\pi-\pi$-stacking interactions in the solid state. They are volatile and decompose at elevated temperatures to give MSe and either $(SeC_6F_5)_2$ or $Se(C_6F_5)_2$.

Introduction

Fluorinated ligands impart unique chemical and physical properties to inorganic compounds, including superior solubility/volatility characteristics, unusual crystal packing motifs, and stabilization of the elements in high oxidation states.[1] There exists an extensive group of fluorinated ligands, including alkyls, aryls, amides, alkoxides, acetonylacetates, carboxylates, phosphine oxides, phosphines, and thiolates. Each ligand class confers unique advantages for the synthesis of compounds with particular chemical or physical properties.

Of the monodentate anions of the group 16 elements, the fluorinated phenoxide OC_6F_5 has been used throughout the periodic chart, in main-group,[2] transition-metal,[3] lanthanide,[4] and actinide[5] chemistry. This phenoxide imparts chemical stability, particularly with metal ions in high oxidation states, and improves solubility properties. The more electropositive metal ions tend to form dative M−F interactions[6] that are interesting as models for understanding the first step in C−F bond activation processes. There is also a tendency of $M(OC_6F_5)_x$ compounds to crystallize in lattices with significant $\pi-\pi$-stacking interactions.

The fluorinated thiolate SC_6F_5 has been used similarly in s-,[7] p-,[8] d-,[9] and f-block[10−13] research, again giving products

*To whom correspondence should be addressed. E-mail: bren@rci.rutgers.edu (J.G.B.), emge@rci.rutgers.edu (T.J.E.).

(1) (a) Willis, C. J. *Coord. Chem. Rev*. **1988**, *88*, 133. (b) Witt, M.; Roesky, H. W. *Prog. Inorg. Chem*. **1992**, *40*, 353. (c) Lentz, D. *Angew. Chem*. **1994**, *106*, 1377. (d) Lentz, D. *J. Fluorine Chem*. **2004**, *125*, 853. (e) Hubert-Pfalzgraf, L. G. *Appl. Organomet. Chem*. **1992**, *6*, 627.

(2) (a) Britovsek, G. J. P.; Ugolotti, J.; White, A. J. P. *Organometallics* **2005**, *24*, 1685. (b) Metz, M. V.; Sun, Y.; Stern, C. L.; Marks, T. J. *Organometallics* **2002**, *21*, 3691. (c) Whitmire, K. H.; Hoppe, S.; Sydora, O.; Jolas, J. L.; Jones, C. M. *Inorg. Chem*. **2000**, *39*, 85. (d) Jolas, J. L.; Hoppe, S.; Whitmire, K. H. *Inorg. Chem*. **1997**, *36*, 3335. (e) Jones, C. M.; Burkart, M. D.; Bachman, R. E.; Serra, D. L.; Hwu, S. J.; Whitmire, K. H. *Inorg. Chem*. **1993**, *32*, 5136.

(3) (a) Tremblay, T. L.; Ewart, S. W.; Sarsfield, M. J.; Baird, M. C. *Chem. Commun*. **1997**, 831. (b) Campbell, C.; Bott, S. G.; Larsen, R.; Van Der Sluys, W. G. *Inorg. Chem*. **1994**, *33*, 4950. (c) Amor, J. I.; Burton, N. C.; Cuenca, T.; Gomez-Sal, P.; Royo, P. *J. Organomet. Chem*. **1995**, *485*, 153. (d) Abbott, R. G.; Cotton, F. A.; Falvello, L. R. *Inorg. Chem*. **1990**, *29*, 514. (e) Dilworth, J. R.; Gibson, V. C.; Redshaw, C.; White, A. J. P.; Williams, D. J. *J. Chem. Soc., Dalton Trans*. **1999**, 2701. (f) Metz, M. V.; Sun, Y.; Stern, C. L.; Marks, T. J. *Organometallics* **2002**, *21*, 3691. (g) Ferreira Lima, G. L.; Araujo Melo, D. M.; Isolani, P. C.; Thompson, L. C.; Zinner, L. B.; Vicentini, G. *Anais Assoc. Brasil. Quim*. **2000**, *49*, 153. (h) Kim, M.; Zakharov, L. N.; Rheingold, A. L.; Doerrer, L. H. *Polyhedron* **2005**, *24*, 1803. (i) Buzzeo, M. C.; Iqbal, A. H.; Long, C. M.; Millar, D.; Patel, S.; Pellow, M. A.; Saddoughi, S. A.; Smenton, A. L.; Turner, J. F. C.; Wadhawan, J. D.; Compton, R. G.; Golen, J. A.; Rheingold, A. L.; Doerrer, L. H. *Inorg. Chem*. **2004**, *43*, 7709.

(4) (a) Norton, K.; Emge, T. J.; Brennan, J. G. *Inorg. Chem*. **2007**, *46*, 4060. (b) Norton, K.; Kumar, G. A.; Dilks, J. L.; Emge, T. J.; Riman, R. E.; Brik, M. G.; Brennan, J. G. *Inorg. Chem*. **2009**, *48*, 4060.

(5) (a) Schnaars, D. D.; Wu, G.; Hayton, T. W. *Dalton Trans*. **2009**, *19*, 3681. (b) Fortier, S.; Wu, G.; Hayton, T. W. *Inorg. Chem*. **2009**, *48*, 3000.

(6) (a) Plenio, H. *Chem. Rev*. **1997**, *97*, 3363. (b) Plenio, H. *ChemBioChem* **2004**, *5*, 650.

(7) Chadwick, S.; Englich, U.; Noll, B.; Ruhlandt-Senge, K. *Inorg. Chem*. **1998**, *37*, 4718.

(8) (a) Peach, M. E. *J. Inorg. Nucl. Chem*. **1973**, *35*, 1046. (b) Peach, M. E. *Can. J. Chem*. **1968**, *46*, 2769. (c) De Mel, V. S. J.; Kumar, R.; Oliver, J. P. *Organometallics* **1990**, *9*, 1303. (d) Hendershot, D. G.; Kumar, R.; Barber, M.; Oliver, J. P. *Organometallics* **1991**, *10*, 1917. (e) Delgado, E.; Hernandez, E.; Hedayat, A.; Tornero, J.; Torre, R. *J. Organomet. Chem*. **1994**, *466*, 119. (f) Estudiante-Negrete, F.; Redon, R.; Hernandez-Ortega, S.; Toscano, R. A.; Morales-Morales, D. *Inorg. Chim. Acta* **2007**, *360*, 1651. (g) Charmant, J. P. H.; Jahan, A. H. M.; Norman, N. C.; Orpen, A. G. *Inorg. Chim. Acta* **2005**, *358*, 1358.

(9) (a) Carlton, L.; Tetana, Z. N.; Fernandes, M. A. *Polyhedron* **2008**, *27*, 1959. (b) Shawakfeh, K.; El-Khateeb, M.; Taher, D.; Goerls, H.; Weigand, W. *Transition Met. Chem*. **2008**, *33*, 387. (c) Rivera, G.; Bernes, S.; Torrens, H. *Polyhedron* **2007**, *26*, 4276. (d) Baldovino-Pantaleon, O.; Rios-Moreno, G.; Toscano, R. A.; Morales-Morales, D. *J. Organomet. Chem*. **2005**, *690*, 2880.

(10) (a) Melman, J.; Emge, T. J.; Brennan, J. G. *Inorg. Chem*. **2001**, *40*, 1078. (b) Melman, J.; Rhode, C.; Emge, T. J.; Brennan, J. G. *Inorg. Chem*. **2002**, *41*, 28.

(11) Kumar, G. A.; Riman, R. E.; Diaz Torrez, L. A.; Garcia, O. B.; Banerjee, S.; Kornienko, A.; Brennan, J. G. *Chem. Mater*. **2005**, *17*, 5130.

(12) Banerjee, S.; Kumar, G. A.; Emge, T. J.; Riman, R. E.; Brennan, J. G. *Chem. Mater*. **2008**, *20*, 4367.

(13) Banerjee, S.; Huebner, L.; Romanelli, M. D.; Kumar, G. A.; Riman, R. E.; Emge, T. J.; Brennan, J. G. *J. Am. Chem. Soc*. **2005**, *127*, 15900.

Published on Web 07/23/2010

with superior solubility properties and leading to the formation of products with distinctive structural characteristics. Most recently, these SC_5F_6 ligands were used to make a series of $(DME)_2Ln(SC_6F_5)_3$ (Ln = Nd,[11] Er,[12] and Tm[13]) coordination complexes that had, at that time, the highest near-infrared (NIR) emission quantum efficiencies ever reported for molecular lanthanide sources. These thiolates are considerably more emissive than the analogous phenoxides[4b] because the low Ln−S stretching frequencies are not as well-matched to the NIR transition energies, whereas the Ln−O vibrations are considerably higher in energy and are more likely to vibrationally quench the excited-state Ln ion.

The analogous fluorinated selenolate chemistry is essentially undeveloped. The SeC_6F_5 ligand is not commercially available as either the selenol or the diselenide, but a reliable synthesis of $C_6F_5Se\text{-}SeC_6F_5$ has been reported.[14] There exists a description of $Tl(SeC_6F_5)$ and heterometallic M/Tl compounds with SeC_6F_5 ligands that contained dative Tl−F interactions,[15] and a *mer*-octahedral lanthanide compound with a significant structural trans influence.[16] $Hg(SeC_6F_5)_2$ has also been prepared by the direct combination of Hg with the diselenide, although no structural characterization details were included.[17]

The fact that there has been no systematic investigation into the chemistry of the group 12 metals (M = Zn, Cd, and Hg) with fluorinated selenolates is surprising, because the same desirable characteristics noted for the phenoxides and thiolates can be expected for the selenolates, and these properties can be exploited in a wide range of disciplines. For example, II−VI materials with fluorinated selenolates will likely show increased solubility in organic matrices, which is potentially important for the doping of selenolate passivated quantum dots[18] into polymers.[19] The often displayed $\pi-\pi$-stacking interactions can potentially lead to new forms of old materials, whether it be new cluster structures[20] or dimensionally restricted solid-state materials.[21] In more ionic chemistry, the Hg derivative would be particularly useful as a transmetalation reagent for connecting SeC_6F_5 ligands with electropositive metals, and Ln/M cluster compounds with fluorinated selenolates should be particularly bright NIR or visible emission sources, because the low-energy M−Se vibration and the reduced number of emission quenching C−H bonds should favor radiative over vibrational relaxation processes. Finally, in chemical vapor deposition, simple $M(SeC_6F_5)_n$ coordination compounds should be more volatile than their hydrocarbon counterparts. For these reasons, we have begun to examine the systematic inorganic chemistry of the fluorinated selenolate ligand and describe here the synthesis, characterization, and thermal decomposition of $M(SeC_6F_5)_2$ (M = Zn, Cd, and Hg).

Experimental Section

General Methods. All syntheses were carried out under ultrapure nitrogen (Welco Praxair), using conventional drybox or Schlenk techniques. Pyridine (Aldrich) was purified with a dual-column Solv-Tek solvent purification system and collected immediately prior to use. $Se_2(C_6F_5)_2$ was prepared according to literature procedures.[14] Zinc (J.T. Baker), cadmium (Aldrich), and mercury (Aldrich) metals were purchased and used as received. Melting points were recorded in sealed capillaries and are uncorrected. IR spectra were recorded on a Thermo Nicolet Avatar 360 FTIR spectrometer from 4000 to 450 cm^{-1} as Nujol mulls on CsI plates. UV−vis absorption spectra were recorded on a Varian DMS 100S spectrometer with the samples dissolved in pyridine, placed in either a 1.0 mm × 1.0 cm Spectrosil quartz cell or a 1.0 cm^2 special optical glass cuvette, and scanned from 190 to 800 nm. ^1H, ^{19}F, and ^{77}Se NMR spectra were obtained on Varian spectrometers. Electrospray ionization mass spectrometry (ESI-MS) data were recorded on a Thermo Finnigan LCQ DUO system with the sample dissolved in a 10:1 $MeOH/CH_3COOH$ mixture. Mass spectra were acquired in the negative-ion detection mode, scanning a mass range from m/z 150 to 1000. In the case of isotopic patterns, the value given is for the most intense peak. Powder X-ray diffraction (PXRD) data were obtained on a Bruker HiStar area detector using Cu Kα radiation from a Nonius 571 rotating-anode generator. Elemental analyses were performed by Quantitative Technologies, Inc. (Whitehouse, NJ).

Synthesis of $(py)_2Zn(SeC_6F_5)_2$ (1). Zn (0.065 g, 0.99 mmol), Hg (0.020 g, 0.099 mmol), and $Se_2(C_6F_5)_2$ (0.492 g, 1.00 mmol) were combined in pyridine (ca. 25 mL), and the mixture was stirred at room temperature for 10 days. The solution was filtered to remove Hg, concentrated to ∼5 mL, and held at −5 °C to give near-colorless laths (0.604 g, 85%) that begin to melt at 154 °C and melt completely at 163 °C. IR: 2921 (s), 2717 (w), 2357 (w), 1605 (m), 1507 (m), 1462 (s), 1372 (s), 1217 (w), 1070 (m), 964 (m), 813 (m), 718 (m), 637 (w), 420 (w) cm^{-1}. UV−vis: This compound gives an optical absorption maximum at 477 nm. Anal. Calcd for $C_{22}H_{10}N_2F_{10}ZnSe_2$: C, 36.9; H, 1.40; N, 3.91. Found: C, 36.7; H, 1.42; N, 3.90. ^1H NMR (399.89 MHz, acetone-d_6; δ, ppm): 7.75 (dt, 2H), 8.22 (tt, 1H), 8.77 (dd, 2H). ^{19}F NMR (376.22 MHz, acetone-d_6; δ, ppm): −121.13 (dd, 2F), −158.55 (t, 1F), −161.02 (tt, 2F). ^{77}Se NMR (76.28 MHz, pyridine-d_5; δ, ppm): 476.6 (s) (vs PhSeSePh at 468.0 ppm as an external standard). ESI-MS: m/z 738 (MNa^+), 494 ($F_5C_6Se\text{-}SeC_6F_5^+$), 247 ($SeC_6F_5^+$).

Synthesis of $(py)_2Cd(SeC_6F_5)_2$ (2). Cd (0.056 g, 0.498 mmol) and $Se_2(C_6F_5)_2$ (0.245 g, 0.498 mmol) were combined in pyridine (ca. 25 mL), and the mixture was stirred at room temperature for

(14) Klapötke, T. M.; Krumm, B.; Polborn, K. *Eur. J. Inorg. Chem.* **1999**, 1359.
(15) Davidson, J. L.; Holz, B.; Leverd, P. C.; Lindsell, W. E.; Simpson, N. J. *J. Chem. Soc., Dalton Trans.* **1994**, 3527.
(16) Krogh-Jespersen, K.; Romanelli, M. D.; Melman, J. H.; Emge, T. J.; Brennan, J. G. *Inorg. Chem.* **2010**, *49*, 552.
(17) (a) Kostiner, E.; Reddy, M. L. N.; Urch, D. S.; Massey, A. G. *J. Organomet. Chem.* **1968**, *15*, 383. (b) Cohen, S. C.; Massey, A. G. *Adv. Fluorine Chem.* **1970**, *6*, 83.
(18) (a) Howes, P.; Green, M.; Johnston, C.; Crossley, A. *J. Mater. Chem.* **2008**, *18*, 3474. (b) Abeykoon, A. M. M.; Castro-Colin, M.; Anokhina, E. V.; Iliev, M. N.; Donner, W.; Jacobson, A. J.; Moss, S. C. *Phys. Rev. B* **2008**, *77*, 075333/1. (c) Kedarnath, G.; Kumbhare, L. B.; Jain, V. K.; Wadawale, A.; Dey, G. K.; Thinaharan, C.; Naveen, S.; Sridhar, M. A.; Prasad, J. S. *Bull. Chem. Soc. Jpn.* **2008**, *81*, 489. (d) Dass, A.; Guo, R.; Tracy, J. B.; Balasubramanian, R.; Douglas, A. D.; Murray, R. W. *Langmuir* **2008**, *24*, 310. (e) Brennan, J. G.; Siegrist, T.; Caroll, P.; Stuczynski, S.; Brus, L.; Steigerwald, M. L. *J. Am. Chem. Soc.* **1989**, *111*, 4141. (f) Brennan, J. G.; Siegrist, T.; Stuczynski, S.; Carroll, P.; Rynders, P.; Brus, L. E.; Steigerwald, M. L. *Chem. Mater.* **1990**, *2*, 403.
(19) (a) Dimitriev, O. P.; Ogurtsov, N. A.; Pud, A. A.; Smertenko, P. S.; Piryatinski, Yu. P.; Noskov, Yu. V.; Kutsenko, A. S.; Shapoval, G. S. *J. Phys. Chem. C* **2008**, *112*, 14745. (b) Aslam, F.; Graham, D. M.; Binks, D. J.; Dawson, P.; Pickett, N.; O'Brien, P.; Byeon, C. C.; Ko, D.-K.; Lee, J. *J. Appl. Phys.* **2008**, *103*, 093702/1. (c) Firth, A. V.; Tao, Y.; Wang, D.; Ding, J.; Bensebaa, F. *J. Mater. Chem.* **2005**, *15*, 4367. (d) Kedarnath, G.; Dey, S.; Jain, V. K.; Dey, G. K.; Varghese, B. *Polyhedron* **2006**, *25*, 2383.
(20) (a) Eichhofer, A.; Hampe, O.; Blom, M. *Eur. J. Inorg. Chem.* **2003**, 1307. (b) Soloviev, V. N.; Eichhoefer, A.; Fenske, D.; Banin, U. *J. Am. Chem. Soc.* **2001**, *123*, 2354. (c) Soloviev, V. N.; Eichhoefer, A.; Fenske, D.; Banin, U. *J. Am. Chem. Soc.* **2000**, *122*, 2673. (d) DeGroot, M. W.; Khadka, C.; Roesner, H.; Corrigan, J. F. *J. Cluster Sci.* **2006**, *17*, 97. (e) Eichhoefer, A. *Eur. J. Inorg. Chem.* **2005**, 1245.
(21) (a) Huang, X.; Li, J. *J. Am. Chem. Soc.* **2007**, *129*, 3157. (b) Huang, X.; Heulings, H. R.; Le, V.; Li, J. *Chem. Mater.* **2001**, *13*, 3754. (c) Huang, X.; Li, J.; Fu, H. *J. Am. Chem. Soc.* **2000**, *122*, 8789. (d) Girgis, S. Y.; Salem, A. M.; Selim, M. S. *J. Phys. B: Condens. Matter Mater. Phys.* **2007**, *19*, 116213/1.

Table 1. Summary of Crystallographic Details for **1**−**4**[a]

	1	2	3	4
empirical formula	$C_{22}H_{10}F_{10}N_2Se_2Zn$	$C_{22}H_{10}F_{10}N_2Se_2Cd$	$C_{12}F_{10}HgSe_2$	$C_{12}H_{10}HgSe_2$
fw	715.61	762.64	692.63	512.71
space group	$P2_1/n$	$P2_1/n$	$P\bar{1}$	$P2_1/c$
a (Å)	9.3073(5)	9.086(3)	14.6756(6)	14.7309(8)
b (Å)	17.0503(9)	23.255(7)	17.8623(9)	5.5967(3)
c (Å)	14.8291(8)	12.034(4)	21.629(2)	7.3167(4)
α (deg)	78.392(3)			
β (deg)	100.020(1)	109.276(6)	83.452(2)	103.399(1)
γ (deg)	77.348(3)			
V (Å^3)	2317.4(2)	2400(1)	5404.5(6)	586.80(6)
Z	4	4	15	2
D(calcd) (g/cm^3)	2.051	2.110	3.192	2.902
temperature (K)	100(2)	100(2)	100(2)	100(2)
λ (Å)	0.710 73	0.710 73	0.710 73	0.710 73
abs coeff (mm^{-1})	4.297	2.145	15.841	19.279
$R(F)^b$ [$I > 2\,\sigma(I)$]	0.0190	0.0438	0.0515	0.0172
$R_w(F^2)^c$ [$I > 2\,\sigma(I)$]	0.0461	0.0842	0.1205	0.0425

[a] Additional crystallographic details are given in the Supporting Information. [b] Definitions: $R(F) = \sum||F_o| - |F_c||/\sum|F_o|$. [c] $R_w(F^2) = \{\sum[w(F_o^2 - F_c^2)^2]/\sum[w(F_o^2)^2]\}^{1/2}$.

1 week. The solution was filtered, concentrated to ∼5 mL, and held at −5 °C to give colorless plates (0.239 g, 63%) that begin to melt at 150 °C and melt completely at 175 °C. IR: 2900 (s), 1602 (m), 1510 (m), 1504 (m), 1462 (s), 1459 (s), 1376 (s), 1264 (w), 1037 (w), 1010 (w), 814 (m), 693 (m), 629 (w), 463 (w) cm^{-1}. This compound does not have an absorption maximum between 320 and 800 nm. Anal. Calcd for $C_{22}H_{10}N_2F_{10}CdSe_2$: C, 34.6; H, 1.32; N, 3.67. Found: C, 34.5; H, 1.51; N, 3.54. ^{1}H NMR (499.77 MHz, DMSO-d_6; δ, ppm): 8.63 (dt, 2H), 7.45 (dt, 1H), 7.25 (m, 2H). ^{19}F NMR (470.25 MHz, DMSO-d_6; δ, ppm): −124.64 (d, 2F), −163.42 (t, 1F), −165.21 (t, 2F).

Synthesis of Hg(SeC$_6$F$_5$)$_2$ (3). Hg (0.100 g, 0.498 mmol) and $Se_2(C_6F_5)_2$ (0.245 g, 0.497 mmol) were combined in pyridine (ca. 25 mL), and the mixture was stirred at room temperature for 1 week. The solution was filtered to remove unreacted Hg and brought to dryness. The solid was washed with hexanes, redissolved in ∼8 mL of toluene, and heated to 60 °C for 30 min before cooling back to room temperature. The solution was then held at −5 °C for 1 week to give colorless needles (0.215 g, 62%) that melt at 115 °C. This melting point is significantly lower than the temperature at which sublimed $Hg(SeC_6H_5)_2$ (**4**) melts, which implies that the two purification techniques lead to different molecular phases.[17] IR: 2850 (s), 1602 (m), 1510 (m), 1504 (m), 1462 (s), 1459 (s), 1376 (s), 1264 (w), 1037 (w), 1010 (w), 814 (m), 693 (m), 629 (w), 463 (w) cm^{-1}. This compound does not have an optical absorption maximum between 320 and 800 nm. Anal. Calcd for $C_{12}F_{10}HgSe_2$: C, 20.8. Found: C, 20.3. ^{19}F NMR (470.25 MHz, DMSO-d_6; δ, ppm): −125.22 (dd, 2F), −158.10 (t, 1F), −162.95 (m, 2F).

Thermolysis of 1−3. A sample of **1** (20 mg) was placed in a quartz thermolysis tube that was sealed under vacuum, and the sample end was placed into a model 847 Lindberg tube furnace. The "cold" end of the glass tube was held at −196 °C by immersion in liquid nitrogen. The sample was heated to 650 °C at a ramp rate of 10 °C/min and then held at 650 °C for 5 h, at which time it was cooled to 25 °C at a rate of 3.5 °C/min. The black powder that was formed at the sample end of the quartz tube was identified as cubic ZnSe[22] (2003 JCPDS card no. 88-2345). A volatile, polycrystalline thermolysis product found at the cold region of the quartz tube was identified as $Se(C_6F_5)_2$ by gas chromatography (GC)−MS.

As was done previously, **2** (10 mg) was heated at 650 °C for 2.2 h. PXRD revealed that the only crystalline phase present was the wurtzite (hexagonal) form of CdSe[23] (2003 JCPDS card no. 77-2307). The volatile product, a yellow crystalline material, was identified as $(SeC_6F_5)_2$ by single-crystal XRD[24] and its melting point.[25]

As was done previously for **1**, **3** (10 mg) deposited a dark powder at the region of the tube furnace where the quartz sample tube exited the alumina furnace tube. The powder was identified as cubic HgSe[26] by PXRD (2003 JCPDS card no. 065-4590), and GC−MS analysis identified the volatile product as $Se(C_6F_5)_2$.

X-ray Structure Determination. Data for **1**−**3** and for Hg(SePh)$_2$ **4** were collected on a Bruker Smart APEX CCD diffractometer with graphite-monochromatized Mo Kα radiation (λ = 0.710 73 Å) at 100 K. Crystals were immersed in paratone oil and examined at low temperatures. The data were corrected for Lorenz effects and polarization and absorption, the latter by a multiscan (*SADABS*)[27] method. The structures were solved by direct methods (*SHELXS86*).[28] All non-H atoms were refined (*SHELXL97*)[29] based upon F_{obs}^2. All H-atom coordinates were calculated with idealized geometries (*SHELXL97*). Scattering factors (f_o, f', f'') are as described in *SHELXL97*. Crystallographic data and final R indices for **1**−**4** are given in Table 1. ORTEP diagrams[30] for **1**−**4** are shown in Figures 1, 3, 5, and 7, respectively. Packing diagrams for **1**−**4** are given in Figures 2, 4, 6, and 8, respectively. Complete crystallographic details are given in the Supporting Information.

Results and Discussion

The group 12 metals all react with $C_6F_5SeSeC_6F_5$ in pyridine over a period of days to weeks. Reactions proceed slowly, and not to completion, in relatively apolar solvents

(22) Lao, P. D.; Gou, Y.; Siu, G. G.; Shen, S. C. *Phys. Rev. B: Condens. Matter Mater. Phys.* **1993**, *48*, 11701.
(23) Freeman, D. K.; Mair, S. L.; Barnea, Z. *Acta Crystallogr., Sect. A* **1977**, *33*, 355.
(24) Woodard, C. M.; Brown, D. S.; Lee, J. D.; Massey, A. G. *J. Organomet. Chem.* **1976**, *121*, 333.
(25) Makarov, A. Y.; Tersago, K.; Nivesanond, K.; Blockhuys, F.; Van Alsenoy, C.; Kovalev, M. K.; Bagryanskaya, I. Y.; Gatilov, Y. V.; Shakirov, M. M.; Zibarev, A. V. *Inorg. Chem.* **2006**, *45*, 2221.
(26) Leute, V.; Plate, H. *Ber. Bunsenges. Phys. Chem.* **1989**, *93*, 757.
(27) Bruker-AXS. *SADABS, Bruker Nonius area detector scaling and absorption correction*, version 2.05; Bruker-AXS Inc.: Madison, WI, 2003.
(28) Sheldrick, G. M. *SHELXS86, Program for the Solution of Crystal Structures*; University of Göttingen: Göttingen, Germany, 1986.
(29) (a) Sheldrick, G. M. *Acta Crystallogr.* **2008**, *A64*, 112. (b) Sheldrick, G. M. *SHELXL97, Program for Crystal Structure Refinement*; University of Göttingen: Göttingen, Germany, 1997.
(30) Graphics programs. ORTEP-3 for Windows: Farrugia, L. J. *J. Appl. Crystallogr.* **1997**, *30*, 565. Burnett, M. N.; Johnson, C. K. ORTEP-III: Oak Ridge Thermal Ellipsoid Plot Program for Crystal Structure Illustrations. Oak Ridge National Laboratory Report ORNL-6895; 1996; Persistence of Vision Pty. Ltd.: Persistence of Vision Raytracer (Version 3.6) 2004.

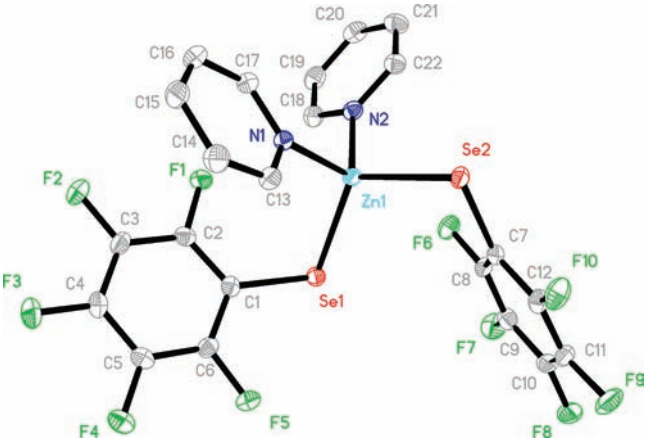

Figure 1. ORTEP diagram of **1** with the H atoms removed for clarity and ellipsoids at the 50% probability level. Significant bond lengths [Å] and angles [deg]: Zn1−N1, 2.055(1); Zn1−N2, 2.060(1); Zn1−Se1, 2.4130(2); Zn1−Se2, 2.4175(3); Se1−C1, 1.905(2); Se2−C7, 1.904(2); N1−Zn1−N2, 105.75(5); N1−Zn1−Se1, 111.01(4); N2−Zn1−Se1, 108.39(4); N1−Zn1−Se2, 103.74(4); N2−Zn1−Se2, 110.45(4); Se1−Zn1−Se2, 116.914(9).

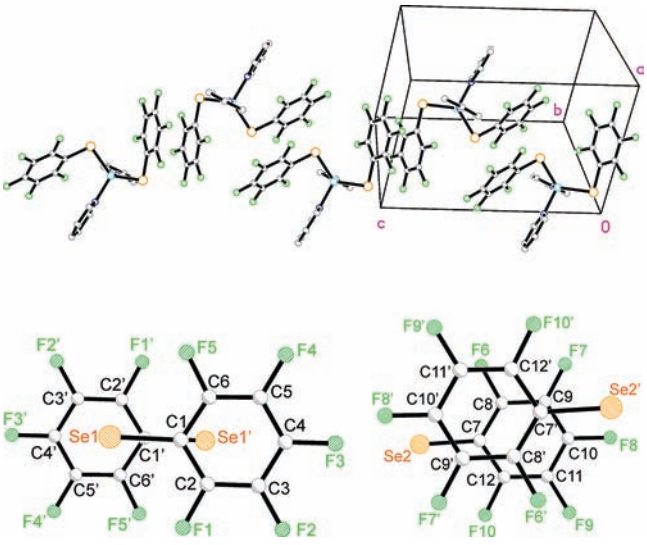

Figure 2. (Top) ORTEP diagram illustrating the 1-D stacking of molecules with $\pi-\pi$ interactions for **1**, viewed approximately along the $a-b$ vector. (Bottom) ORTEP diagrams of close-ups of two distinct ring$\cdots$ring interactions for adjacent and coparallel rings in $(py)_2Zn(SeC_6F_5)_2$ viewed normal to the phenyl rings.

such as toluene or tetrahydrofuran (THF), but in pyridine the metals dissolve completely [reaction (1)], and extraction of the product with toluene, followed by saturation, gives high yields of $M(SeC_6F_5)_2$.

$$M + C_6F_5SeSeC_6F_5 \rightarrow (py)_xM(SeC_6F_5)_2$$
$$(M = Zn \text{ or } Cd,\ x = 2;\ M = Hg,\ x = 0) \qquad (1)$$

Low-temperature single-crystal XRD of the Zn and Cd compounds shows that they crystallize as the pyridine adducts **1** and **2**, while the Hg compound **3** crystallizes without

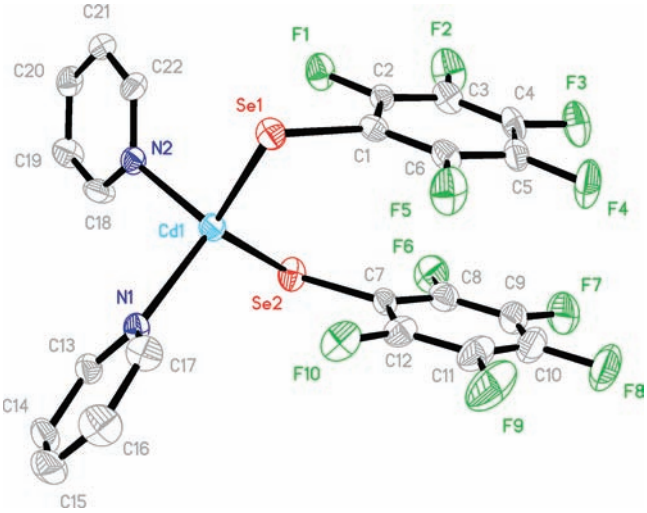

Figure 3. ORTEP diagram of **2** with the H atoms removed for clarity and ellipsoids at the 30% probability level. Selected Bond lengths [Å] and angles [deg]: Cd1−N1, 2.286(5); Cd1−N2, 2.289(4); Cd1−Se1, 2.5645(9); Cd1−Se2, 2.596(1); Se1−C1, 1.902(6); Se2−C7, 1.901(6); N1−Cd1−N2, 105.8(2); N1−Cd1−Se1, 110.5(1); N2−Cd1−Se1, 109.9(1); N1−Cd1−Se2, 111.3(1); N2−Cd1−Se2, 95.07(1); Se1−Cd1−Se2, 122.15(3).

pyridine, giving a complicated structure with two short Hg−Se bonds and an array of significantly longer Hg−Se interactions. The Hg-containing compound is similar in molecular structure to, but quite different in crystal packing motif from, **4**. The structure of **4** had been reported[31] to have molecules on 2-fold sites of the C-centered C2 cell, but our analysis of weak- and intermediate-intensity X-ray reflections revealed that the true lattice was primitive and centrosymmetric and that the true site symmetry of the molecule **4** was inversion. The molecular structures of **1**−**4** are shown in Figures 1, 3, 5, and 7, respectively, with significant bond geometries for **1** and **2** given in the figure captions and selected bonding and nonbonding geometries for **3** listed in Table 2.

The Zn compound **1** (Figure 1) has a slightly distorted tetrahedral coordination with a wide range of ligand−Zn−ligand angles (105.8−116.9°, average 109.3°). There are two statistically equivalent Zn−N bond lengths of 2.058(1) Å that are typical for Zn−pyridine interactions, and there are two nearly equal Zn−Se bond lengths [2.4130(2) and 2.4175(3) Å] that are also within the normal range found for Zn−Se bonds found in the Cambridge Structural Database (CSD).[41] A pair of similar $(py)_2Zn(SeR)_2$ compounds in the literature affords an opportunity to evaluate the effect of fluorination on the Zn−Se bond length: in $(3,5\text{-}Me_2\text{-}C_5H_3N)_2Zn(SeSiMe_3)_2$[32] [Zn−Se = 2.396(2) Å; Zn−N = 2.10(1) Å] and $(py)_2Zn(SeC_6H_2Me_3\text{-}2,4,6)_2$ [Zn−Se = 2.377(1) Å; Zn−N = 2.118(4) Å],[33] the Zn−Se bonds are all slightly but significantly shorter than the Zn−Se bond lengths found in **1**, which would be consistent with a higher degree of polarization of the electron density away from the Zn−Se bond in **1**.

There is no evidence for any significant Zn−F interaction (closest intramolecular Zn$\cdots$F is for F6 at 2.98 Å; closest intermolecular Zn$\cdots$F is for F8;1 + x, y, z at 3.55 Å), but there are clearly defined $\pi-\pi$-stacking interactions present in

(31) Lang, E. S.; Dias, M. M.; Abram, U.; Vazquez-Lopez, E. M. *Z. Anorg. Allg. Chem.* **2000**, *626*, 784. The synthesis of 4 is described in this reference. Unfortunately, the authors appear to have missed the weak primitive lattice reflections in their crystallographic analysis, giving rise to erroneous molecular and crystal structures.

(32) Azad, M.; Malik, M.; Motevalli, M.; O'Brien, P. *Polyhedron* **1999**, *18*, 1259.

(33) DeGroot, M. W.; Corrigan, J. F. *Organometallics* **2005**, *24*, 3378.

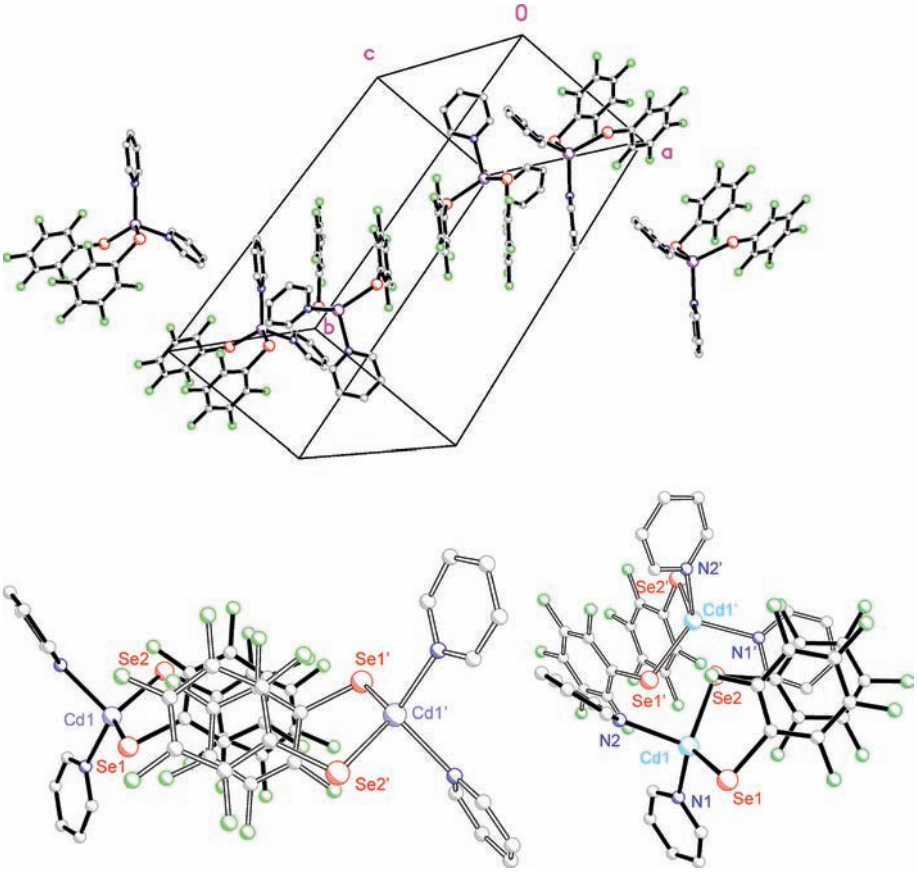

Figure 4. (Top) ORTEP diagram illustrating the isolated stacking of four pentafluorophenyl rings and two pyridine rings indicating $\pi-\pi$ interactions for **2**. (Bottom) ORTEP diagram of the intramolecular $\pi-\pi$ interactions for two adjacent pairs of C_6F_5 rings (e.g., three consecutive interplanar separations of about 3.5 Å) in the crystal structure of **2**. The view is perpendicular to the phenyl ring bonded to Se1. (Left) Related molecules are x, y, z (solid bonds) for that containing Se1 and $1-x, -y, 1-z$ (open bonds and above) for Se1′. (Right) Related molecules are x, y, z (solid bonds) for Se2 and $1-x, -y, 2-z$ (open bonds and below) for Se2′.

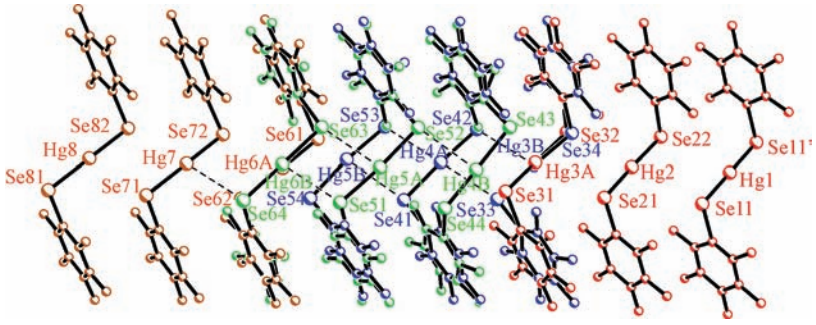

Figure 5. ORTEP diagram of adjacent 1-D arrays of **3** viewed approximately along the crystallographic b^* axis. The horizontal direction is along the crystallographic $b-3c$ direction. The $\pi-\pi$ interactions between C_6F_5 rings are possible along the 1-D array shown as well as between adjacent arrays. The treatment of site disorder by use of a four-part model is demonstrated here by the separate colors of each part (see the text). The shortest Hg···Se contacts (< 3.35 Å) to adjacent molecules are indicated by dashed lines (see Table 2).

the solid state (Figure 2). While there are no *intra*molecular $\pi-\pi$ interactions and no $\pi-\pi$ interactions involving the pyridine ligands, there are two distinct types of *inter*molecular packing interactions between the fluorinated phenyl rings of two adjacent molecules, namely, those related by the inversion center at ($^1/_2$, 0, $^1/_2$) or ($^1/_2$, 0, 1) for rings bonded to Se1 or Se2, respectively (Figure 2). In one case, there is the more direct $\pi-\pi$ interaction with the Se atoms distant to the rings, and in the other case, there is the familiar Se over the ring motif observed in other aromatic selenido compounds including the selenofulvalenes. Because the SeC_6F_5 ligands are located on approximately opposite sides of the molecule (e.g., no close intramolecular association of SeC_6F_5 ligands), the $\pi-\pi$ (or Se···ring) interactions in **1** allow for a 1-D arrangement of closely interacting molecules along the crystallographic c axis. The *SHELXL* mean-plane calculations for the phenyl ring of SeC_6F_5 in **1** yielded plane−plane separations of 3.458(4) and 3.373(5) Å between planes containing Se1 and its inversion symmetry neighbor, Se1′, and Se2 and its inversion symmetry neighbor, Se2′, respectively. In addition, these $\pi-\pi$ interaction distances apparently include the steric effects of the Se atoms but to different

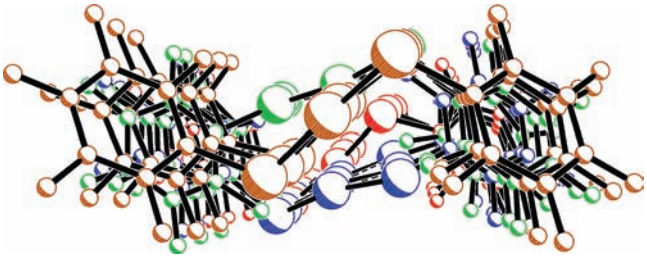

Figure 6. ORTEP diagram of the projection of all 12 component molecules modeled in the *SHELXL* refinement of **3** viewed along the crystallographic $b-3c$ vector, indicating several sites for Hg and Se (larger spheres), despite the generally consistent placement of the C_6F_5 group for nearest-neighbor molecules.

degrees for Se1 and Se2, which are 0.04 and 0.01 Å further away from their respective mean planes. The shift (or linear offset) of rings containing Se1 and Se1′ is ~1.9 Å greater than that for the rings containing Se2 and Se2′ and places atom Se1′ directly above the ring of Se1 (see Figure 2). The combination of wider separation between the rings, greater out-of-plane distance, and positioning of Se1′ above the ring of Se1 indicates that this Se···ring interaction is not likely attractive and more likely a result of steric considerations of the nearby Se1′ atom.

The Cd compound **2** (Figure 3) also contains a similarly distorted tetrahedral metal ion ligand−Cd−ligand angle with a broad range of 95−122° (average 109.1°). There are two pyridine donors with statistically equivalent Cd−N bond lengths [2.288(5) Å] that are within the range found for Cd−pyridine interactions.[34,41] The location of the Cd atom is significantly displaced from either of the mean pyridine planes in the Cd complex, with separations of 0.165(8) and 0.414(8) Å, respectively, to the py1 and py2 planes. This situation contrasts with the very small separations in the Zn complex, at 0.089(2) and 0.038(2) Å, respectively. Such displacements are not unusual for monomeric pyridine complexes of large metals but are in contrast to the values for the smaller Zn metal complex here. Also, as was found for the Zn structure, the two Cd−Se bond lengths are slightly different: Cd1−Se1 = 2.564(1) Å and Cd1−Se2 = 2.596(1) Å. The only related CdN_2Se_2 complex that has been structurally characterized in the literature is (bpy)Cd($SeC_6H_2{}^iPr_3$-2,4,6)$_2$ [Cd−Se = 2.553(4) Å; Cd−N = 2.33(1) Å],[35] and the M−Se bonds in **2** are significantly longer than the Cd−Se bonds in the bpy compound. This could be a result of the steric requirements of the bpy ligand in that complex, or, more likely, the longer Cd−Se bonds in **2** are a result of the polarizing influence of the fluorine substituent.

There is no evidence for any Cd−F interaction in **2**, with shortest intra- and intermolecular Cd···F distances of 3.03 (to F10; x, y, z) and 4.30 Å (to F6; $x, -y+{}^1/_2, z+{}^1/_2$), respectively, but there are both *intra*- and *inter*molecular $\pi-\pi$ interactions present in the solid-state structure of **2** (Figure 4). The intramolecular $\pi-\pi$ interaction is between the two selenolate rings and has a centroid-to-centroid distance of 3.64(1) Å. These two rings are not required by symmetry to be parallel, and they have a small 8.9(4)° dihedral. Other noteworthy distances within this intramolecular $\pi-\pi$ interaction are C6···C12 at 3.412(8) Å and C3···C8 at 3.798(9) Å. The

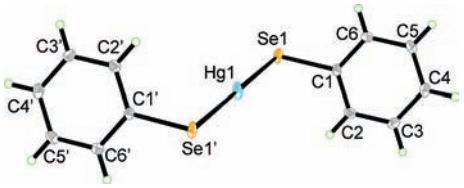

Figure 7. ORTEP diagram of **4** with the ellipsoids at the 50% probability level for non-H atoms. Significant bond lengths [Å] and angles [deg]: Hg1−Se1, 2.4802(2); Hg1−Se1′, 2.4802(2); Se1−C1, 1.922(2); Se1−Hg1−Se1′, 180.0.

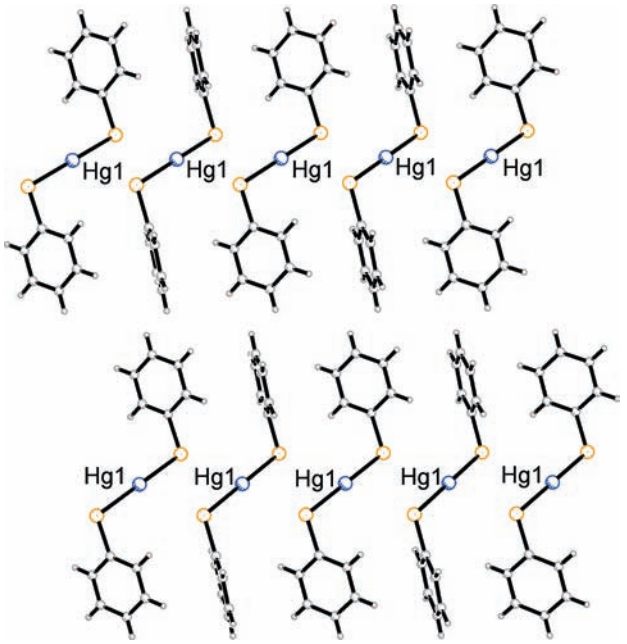

Figure 8. ORTEP diagram of adjacent 1-D arrays of **4** viewed approximately along the crystallographic $b + c$ diagonal axis. The horizontal direction is along the crystallographic $b - c$ direction. The top and bottom arrays are related by inversion through the point (0, ${}^1/_2$, ${}^1/_2$). The $\pi-\pi$ interactions between C_6F_5 rings in **3** are not possible here, owing to the near-perpendicular relationship between adjacent aromatic (Ar) rings. Only H···Ar interactions are possible.

two distinct intermolecular $\pi-\pi$ interactions of **2** are found on either side of the intramolecular $\pi-\pi$ interaction and involve inversion-related Se1 selenolate rings [with a 3.774(1) Å centroid-to-centroid distance] or the Se2 selenolate ring and the N1 pyridine ring of a third molecule [30.2(2)° dihedral and 3.583(1) Å centroid-to-C16′ and 3.460(1) Å C7···C17′ distances, as in Figure 4]. Beyond the N1 pyridine ring, the N2 pyridine of a fourth molecule appears to terminate the stacking of several of these rings along the crystallographic $a-c$ direction, with the perpendicular H21···N1 interaction distance of 2.93 Å between pyridine rings that have a 82.4(1)° dihedral. Because there is inversion symmetry, there are a total of eight rings that are involved in the "pocket" of $\pi-\pi$ interactions, as shown in Figure 4. In summary, the interaction distances between neighboring or approximately parallel rings for **2** are in the range 3.4−3.8 Å, which is consistent with many aromatic ligand metal complexes in the literature.[36,41] Unlike the pure

(34) Hu, C.; Li, Q.; Englert, U. *Cryst. Eng. Commun.* **2003**, *5*, 519.
(35) Subramanian, R.; Givindaswamy, N.; Santos, R. A. *Inorg. Chem.* **1998**, *37*, 4929.

(36) (a) Reger, D. L.; Horger, J.; Smith, M. D.; Long, G. J. *Chem. Commun.* **2009**, *41*, 6219. (b) Corona-Rodriguez, M.; Hernandez-Ortega, S.; Valdes-Martinez, J.; Morales-Morales, D. *Supramol. Chem.* **2007**, *19*, 579. (c) Sonoda, Y.; Goto, M.; Tsuzuki, S.; Tamaoki, N. *J. Phys. Chem. A* **2007**, *111*, 13441.

Table 2. Selected Hg−Se Bond and Hg···Se Contact Lengths [Å] and Angles [deg] for **3**[a]

Intramolecular			
Hg1−Se11	2.4623(5)	Hg4B−Se44	2.490(3)
Hg1−Se11′	2.4623(5)	Hg4B−Se43	2.494(3)
Hg2−Se21	2.4674(5)	Hg5A−Se51	2.4859(6)
Hg2−Se22	2.4685(5)	Hg5A−Se52	2.5162(6)
Hg3A−Se31	2.4661(7)	Hg6B−Se64	2.4793(7)
Hg3A−Se32	2.4848(6)	Hg6B−Se63	2.4796(8)
Hg3B−Se33	2.466(1)	Hg6A−Se61	2.459(1)
Hg3B−Se34	2.473(1)	Hg6A−Se62	2.490(1)
Hg4A−Se42	2.4797(5)	Hg7−Se72	2.4702(6)
Hg4A−Se41	2.5006(5)	Hg7−Se71	2.4737(5)
Hg5B−Se53	2.479(1)	Hg8−Se81	2.4656(5)
Hg5B−Se54	2.507(1)	Hg8−Se82	2.4703(5)
Se11−Hg1−Se11′	180.0	Se44−Hg4B−Se43	161.46(12)
Se21−Hg2−Se22	175.44(1)	Se51−Hg5A−Se52	168.65(2)
Se31−Hg3A−Se32	173.16(2)	Se64−Hg6B−Se63	171.37(2)
Se33−Hg3B−Se34	177.91(4)	Se61−Hg6A−Se62	170.42(4)
Se42−Hg4A−Se41	169.77(2)	Se72−Hg7−Se71	173.04(2)
Se53−Hg5B−Se54	169.16(3)	Se81−Hg8−Se82	177.67(1)
Intermolecular and Orthogonal to the Hg−Se Bond (Estimated Standard Deviation Range 0.001−0.003 Å)			
Hg1−Se22	3.704(1)	Hg4B−Se52	**3.267(2)**
Hg1−Se22′	3.704(1)	Hg5A−Se44	3.660(3)
Hg2−Se11	3.739(1)	Hg5A−Se63	**3.299(2)**
Hg2−Se32	3.643(1)	Hg6B−Se51	**3.281(1)**
Hg3A−Se21	3.809(1)	Hg6A−Se72	3.678(1)
Hg3B−Se42	**3.287(1)**	Hg7−Se62	**3.312(1)**
Hg4A−Se33	**3.204(2)**	Hg7−Se82	3.800(1)
Hg4A−Se53	**3.251(2)**	Hg8−Se71	3.662(1)
Hg5B−Se41	**3.340(1)**	Hg8−Se81″	3.730(1)
Intermolecular Angles with Hg and Se (Estimated Standard Deviation Range 0.02−0.1°)			
Se11−Hg1−Se22	88.4	Se43−Hg4B−Se52	92.5
Se11′−Hg1−Se22	91.6	Hg4B−Se44−Hg5A	87.8
Se11−Hg1−Se22′	91.6	Se51−Hg5A−Se63	80.3
Se11′−Hg1−Se22′	88.4	Se52−Hg5A−Se63	97.7
Se22−Hg1−Se22′	180.0	Se51−Hg5A−Se44	98.8
Hg1−Se11−Hg2	91.6	Se52−Hg5A−Se44	81.4
Se21−Hg2−Se32	91.3	Se63−Hg5A−Se44	171.2
Se22−Hg2−Se32	91.8	Hg5A−Se51−Hg6B	99.3
Se21−Hg2−Se11	89.3	Hg5A−Se52−Hg4B	96.6
Se22−Hg2−Se11	87.5	Se64−Hg6B−Se51	96.5
Se32−Hg2−Se11	179.4	Se63−Hg6B−Se51	80.8
Hg2−Se21−Hg3A	88.8	Hg6B−Se63−Hg5A	98.9
Hg2−Se22−Hg1	92.4	Se61−Hg6A−Se72	90.5
Se31−Hg3A−Se21	89.2	Se62−Hg6A−Se72	81.9
Se32−Hg3A−Se21	87.3	Hg6A−Se62−Hg7	97.9
Hg3A−Se32−Hg2	92.4	Se72−Hg7−Se62	90.3
Se33−Hg3B−Se42	78.9	Se71−Hg7−Se62	93.8
Se34−Hg3B−Se42	102.6	Se72−Hg7−Se82	88.7
Hg3B−Se33−Hg4A	101.5	Se71−Hg7−Se82	86.8
Se42−Hg4A−Se33	80.4	Se62−Hg7−Se82	175.9
Se41−Hg4A−Se33	99.0	Hg7−Se71−Hg8	93.1
Se42−Hg4A−Se53	99.3	Hg7−Se72−Hg6A	89.4
Se41−Hg4A−Se53	81.0	Se81−Hg8−Se71	91.6
Se33−Hg4A−Se53	178.0	Se82−Hg8−Se71	90.0
Hg4A−Se41−Hg5B	97.8	Se81−Hg8−Se81″	87.9
Hg4A−Se42−Hg3B	99.0	Se82−Hg8−Se81″	90.5
Se53−Hg5B−Se41	79.5	Se71−Hg8−Se81″	179.0
Se54−Hg5B−Se41	96.8	Hg8−Se81−Hg8″	92.1
Hg5B−Se53−Hg4A	100.6	Hg8−Se82−Hg7	89.9
Se44−Hg4B−Se52	90.3		

[a] Symmetry transformations used to generate equivalent atoms: ′, $-x, -y, -z$; ″, $-x, -y-1, -z+3$.

1-D $\pi-\pi$ stacking of molecules in the crystal structure of **1** via selenolate ligands on opposing sides of the molecule (see Figure 2), the stacking of molecules in the crystal structure of **2** is via the pair of selenolates on one side of the molecule **2** and the N1 pyridine on the opposite side. Also, because the selenolate interactions are in two directions, i.e., toward the inversion-related selenolate *and* the N1 pyridine of a third molecule, the overall $\pi-\pi$ interaction motif is 3-D, with sheets

of closely interacting rings in the crystallographic *ac* plane linked via the selenolate and N1 pyridine "arms" of one molecule extending along the + and − *c* axis.

The Hg-containing compound **3** is chemically distinct from **1** and **2** in that it crystallizes without coordinated pyridine (Figure 5). A similar situation is found for the nonfluorinated relative of **3**, namely, **4** (Figure 7). The aromatic selenolates are on either side of the Hg atom in both cases with Se−Hg−Se angles at or near 180°. The only other compound in the CSD to have aromatic selenolates bonded to a metal (divalent or other) with a ∼180° Se−M−Se angle is $(py)_4Yb(SeC_6H_5)_2$.[37,41] One of the molecules in **3** has the same inversion site symmetry as that of the single molecule in **4**, and this conformation can be considered a trans motif, with inversion-related rings extending away from the Se atoms at near right angles and the extended C−Se···Se−C torsion angle at 180°. The other seven unique molecules in **3** deviate from this trans motif by different degrees (see below).

The crystal structure of **3** is comprised of 1-D arrays of molecules that stack approximately along the crystallographic *b*−3*c* direction, which is the approximate view direction in Figure 6, with nearly constant spacing of ∼3.6 Å between centers of mass of the nearly parallel pentafluorophenyl rings of adjacent molecules (Figure 5). In this motif, $\pi-\pi$ interactions are found for all C_6F_5 rings within the array, but not between arrays, and their geometries fluctuate in a way that is consistent with variation in the intramolecular C−Se···Se−C torsional (or in-plane rotational) angles from one molecule to the next for the eight unique molecules within the 1-D array while maintaining nearly coparallel SeC_6F_5 planes. This situation is in contrast to **1**, **2**, and **4**, which have only one unique molecule per unit cell, and additionally contrasting to **1** where the two SeC_6F_5 planes are not coparallel. As a result, there are significant local variations in the Hg and Se atom positions about the average linear arrangement of the central Se−Hg−Se atoms, as shown by the projection of all eight unique molecules along the 1-D array direction in Figure 6.

The local variations of the Hg and Se atoms in adjacent molecules of **3** allow for some close Hg···Se interactions between pairs of molecules in two orthogonal directions approximately perpendicular to the Hg−Se bond, so that the coordination environment of the Hg atom in these cases appears to be square-planar, as detailed in Table 2. Specifically, for the 12 complete or disordered molecules modeled within the extended 1-D array, there are 18 intermolecular Hg···Se distances in the range 3.20−3.81 Å, eight of which are considered close (e.g., < 3.35 Å). Between adjacent molecular arrays in the crystallographic *bc* plane and between those separated by the crystallographic *a* axis, there are no Hg···Se bonds less than 3.8 Å, in agreement with the 1-D characteristic of the arrays.

The periodicity of the unit cell of **3** reported here is also consistent with a $1c \times 3b \times 5a$ supercell of the $a' = 4.223$ Å, $b' = 5.911$ Å, $c' = 14.495$ Å, $\alpha' = 79.122°$, $\beta' = 85.09°$, and $\gamma' = 85.823°$ modulated structure with space group $P\overline{1}(abg)0$ and single **q** vector $(-0.129a'^* + 0.339b'^* + 0.330c'^*)$ that is nearly commensurate (i.e., $-2/15a'^*$, $1/3b'^*$, $1/3c'^*$). Satellite reflections of up to fourth-order were quite intense, allowing for either the modulated structure or supercell approach for refining the structure. The (3D+1) formalism of the above-described modulation was used in the program *JANA2006* to model the unique $Hg_{0.5}SeC_6F_5$ unit[38] but failed to produce realistic values for the highly correlated modulation, the heavy-atom ADP parameters, and the several disordered sites of the Hg and Se atoms. However, refinement of the 15 molecules in the supercell unit cell described here proceeded with apparently only minor detrimental correlation effects, which were overcome by the use of appropriate restraints of ADP parameters in the refinement program *SHELXL*.[29]

Because of spatial overlap of the component molecules of partially occupied sites, the geometries of all molecules in **3** were restrained in the least-squares refinement by the requirement of similar bonds and angles for the rigid SeC_6F_5 groups (*SHELXL* instruction SAME) and the atomic displacement parameters were restrained to be nearly isotropic (*SHELXL* instructions ISOR, DELU, and SIMU). In the present model, there are not only the two crystallographic inversion centers of the triclinic cell (see Table 1) at (0, 0, 0) and (0, 0.5, 0.5) but also a noncrystallographic inversion center at approximately (1.00, 0.77, 0.70) or in between atoms Hg4A and Hg5A. As a result of the noncrystallographic symmetry, large correlations between nearly equivalent molecules of the four completely occupied and eight partially occupied sites exist. The intermolecular geometries of all molecules are best described by four parts, each with three molecules (of various occupancies that sum to 15 per unit cell). These parts are (1) molecules in the vicinity of the inversion center at (0, 0, 0), represented by the red molecules of Figure 5, (2) molecules in the vicinity of the inversion center at (0, 0.5, 0.5), represented by the orange molecules of Figure 5, (3) molecules on one side of the pseudoinversion center, represented by the blue molecules of Figure 5, and (4) molecules on the other side of the pseudoinversion center, represented by the green molecules of Figure 5. As a result, intermolecular geometries are only defined for adjacent molecules within each of the four parts, namely, (1) Hg3A, Hg2, Hg1, Hg2′, Hg3A′, (2) Hg6A, Hg7, Hg8, Hg8′, Hg7′, Hg6A′, (3) Hg3B, Hg4A, Hg5B, and (4) Hg4B, Hg5A, Hg6B, where primed atoms in parts 1 and 2 are related by crystallographic inversion symmetry and the molecules in part 3 versus part 4 are related to each other by the pseudoinversion symmetry. Noteworthy intra- and intermolecular geometries are described by the distances and angles in Table 2. On the basis of a search of the CSD,[41] typical "short" intermolecular Hg···Se and Hg···F interactions would have distances of less than 3.8 and 3.0 Å, respectively, compared to formal Hg−Se and Hg−F bonds of less than 3.0 and 2.7 Å, respectively. For the Hg···Se contact distances within the structure of **3**, there are eight less than 3.35 Å, and these are indicated by dashed lines in Figure 5. There are no Hg···F contacts shorter than 3.20 Å, except for Hg5A····F35B, which may be as short as 2.80 Å but is not clearly known because the occupancy of the group containing the F35B atom was refined to only 7%. By use of these four parts, the unusual modulation of the occupancies of the eight molecules is also adequately managed in the superstructure model used here, with freely refined occupancies of pairs of components, e.g., Hg3A and Hg3B,

(37) Brewer, M.; Khasnis, D.; Buretea, M.; Berardini, M.; Emge, T. J.; Brennan, J. G. *Inorg. Chem.* **1994**, *33*, 2743.

(38) Petricek, V.; Dusek, M.; Palatinus, L. *JANA2006. The crystallographic computing system*; Institute of Physics: Praha, Czech Republic, 2006. Further calculations on the modulation of 3 are in preparation for *Acta Crystallogr.*

Hg4A and Hg4B, Hg5A and Hg5B, and Hg6A and Hg6B, summing to unity, as expected here. Further calculations of the modulated model using *JANA2006* with new descriptions of the modulation of occupancies and the use of crenels for the disordered molecular sites are the subject of a future report.[38]

The molecular structure of **4** has three features that are quite similar to those of **3**, namely, (A) a linear Se−Hg−Se arrangement, with a 180° angle, (B) two short Hg−Se bonds, both at 2.480 Å, and (C) two pairs of close Hg···Se interactions nearly perpendicular to the Hg−Se molecular vector, at 3.38 and 3.56 Å. For comparison, the nearly linear Se−Hg−Se central atoms in **3** have angles that range from 168 to 180° (average 173°) and Hg−Se bond lengths that range from 2.46 to 2.52 Å (average 2.48 Å) and the Hg···Se contacts orthogonal to the Hg−Se bonds in **3** are desribed above and in Table 2. However, **4** is distinctly *dissimilar* to **3** in its crystal packing motif. This difference is the direct result of the nonparallel arrangement of two adjacent $Hg(SePh)_2$ molecules, with respect to the 54.5° dihedral angle between C_6H_5 rings (Figure 7), in stark contrast to all C_6F_5 rings in **3**, which are approximately parallel to each other (Figure 5). Thus, the nonparallel arrangement of the phenyl rings in **4** prohibits $\pi-\pi$ interactions but allows 2-D interactions of the type H···Ar, resulting in an ordered subcell of the $Hg_{0.5}$-(SePh) unit, while the parallel and 1-D arrangement of C_6F_5 rings in **3** permits rather direct $\pi-\pi$ interactions, but at the expense of requiring a 15-fold supercell for the overall crystallographic periodicity.

The chelating pyridine selenolate $Hg(Se\text{-}2\text{-}NC_5H_4)_2$ has similar structural characteristics,[39] with a linear arrangement of two short Hg−Se bonds [2.458(1) Å] and two orthogonal Hg−Se bonds that are considerably longer, at 3.435(1) Å. In $Hg(Se\text{-}2\text{-}NC_5H_4)_2$, the chelating pyridine N donors complete an octahedral distribution of donor atoms. Again, in **3** the Hg···Se distances (Table 2) are slightly longer than (although often statistically equal to) the comparable molecular Hg−Se bonds in the literature. These weak/versus/strong interactions are also found in the high-pressure (NaCl-like) phase of HgSe, in which there are two short [2.541(4) Å] Hg−Se bonds and two pairs of longer [2.891(4) and 3.2409(5) Å] Hg···Se interactions.[40]

The compounds **1**−**3** are significantly more volatile than their hydrocarbon counterparts and, in particular, the Hg derivative sublimes quantitatively at 120 °C and decomposes at elevated temperatures to give HgSe. The Zn and Cd compounds are less volatile, but heating under vacuum still results in substantial sublimation and eventual decomposition to give MSe. This contrasts directly with earlier work on fluorinated thiolates, where $M(SC_6F_5)_2$ (M = Zn and Cd) were shown to deliver both MF_2 and MSe phases upon thermolysis.[8] The difference in reactivity can be understood by considering the relative bond strengths involved. The C−Se bond in the selenolate is substantially weaker than the C−S bond in the thiolate, and so cleavage to give MSe should occur more readily at the relatively low temperatures necessary to effect thermal decomposition.

Conclusion

The fluorinated selenolate ligand SeC_6F_5 forms stable divalent compounds with the group 12 metals Zn, Cd, and Hg. Coordination compounds isolated from pyridine solvents have either tetrahedral (Zn and Cd) or nearly linear (Hg) geometries, and there are significant $\pi-\pi$-stacking interactions evident throughout all structures. In contrast to the analogous fluorinated thiolate compounds, these selenolates all decompose at elevated temperatures to give solid-state MSe and as such are promising reagents for delivering new forms of II−VI materials.

Acknowledgment. We acknowledge support of the NSF (Grant CHE-0747165). We also thank Vaclav Petricek for his own calculations and advice on the refinement of the $Hg_{0.5}SeC_6F_5$ model within the modulated 3D+1 formalism of *JANA2006*.

Supporting Information Available: X-ray crystallographic files in CIF format for the crystal structures of **1**−**4**. This material is available free of charge via the Internet at http://pubs.acs.org.

(39) Cheng, Y.; Emge, T. J.; Brennan, J. G. *Inorg. Chem.* **1994**, *33*, 3711.
(40) Nelmes, R. J.; McMahon, M. I.; Belmonte, S. A. *Phys. Rev. Lett.* **1997**, *79*, 3668.
(41) Allen, F. H. *Acta Crystallogr.* **2002**, *B58*, 380.